Susitna-Watana Hydroelectric Project Document
ARLIS Uniform Cover Page

Title: Ice processes in the Susitna River study, Study plan Section 7.6, 2014 Study Implementation Report, Appendix C, River2D open-water modeling report, Focus Area 128 (Slough 8A)	**SuWa 289**
Author(s) – Personal:	
Author(s) – Corporate: HDR Alaska, Inc.	
AEA-identified category, if specified: November 2015; Study Completion and 2014/2015 Implementation Reports	
AEA-identified series, if specified:	
Series (ARLIS-assigned report number): Susitna-Watana Hydroelectric Project document number 289	**Existing numbers on document:**
Published by: [Anchorage : Alaska Energy Authority, 2015]	**Date published:** October 2015
Published for: Alaska Energy Authority	**Date or date range of report:**
Volume and/or Part numbers: Study plan Section 7.6	**Final or Draft status, as indicated:**
Document type:	**Pagination:** iii, 29 pages
Related works(s): See below for list. Be aware that the name of the study at the beginning of title varies in each part.	**Pages added/changed by ARLIS:**
Notes: Accompanying volumes (each appears in a separate electronic file): • Ice processes in the Susitna River study, Study plan Section 7.6, 2014-2015 Study Implementation Report. [Main report] • Appendix A. Alternative visualizations of freeze-up progression and open leads. • Appendix B. Technical memorandum: River1D model--initial open water calibration and validation.	

All reports in the Susitna-Watana Hydroelectric Project Document series include an ARLIS-produced cover page and an ARLIS-assigned number for uniformity and citability. All reports are posted online at http://www.arlis.org/resources/susitna-watana/

ARLIS
Alaska Resources Library & Information Services

SUSITNA-WATANA HYDRO

Susitna-Watana Hydroelectric Project (FERC No. 14241)

Ice Processes in the Susitna River Study
Study Plan Section 7.6

2014 Study Implementation Report

Appendix C
River2D Open-Water Modeling Report
Focus Area 128 (Slough 8A)

Prepared for

Alaska Energy Authority

SUSITNA-WATANA HYDRO

Clean, reliable energy for the next 100 years.

Prepared by

HDR Alaska, Inc.

October 2015

TABLE OF CONTENTS

LIST OF TABLES

LIST OF FIGURES

1 INTRODUCTION

Several Focus Areas determined in conjunction with the Instream Flow Studies (Studies 8.5-8.6) in the Middle River were to receive more detailed ice modeling and observation attention. For up to 10 complex and important fish habitat areas containing a variety of main channel, off channel, and side slough areas, River2D models were to be developed, and observations of ice-cover progression, ice thickness, and open leads were to be more detailed in order to calibrate these models. See the Instream Flow Study (RSP Section 8.5) for criteria and potential sites.

2 STUDY AREA

FA-128 (Slough 8A) is located in the Middle River reach of the Susitna River between the mouth of Skull Creek at PRM 128.1 to PRM 130.5. This important salmon habitat area includes several side channels, sloughs, and warmer water upwelling locations conducive to spawning and rearing. Depending on the stage in the main channel, colder river water may or may not flow into the side channels and sloughs. Some sloughs may be fed by groundwater or by flow through the bed and bars of the main channel and into the side channels and sloughs. When the main channel freezes over in the winter, there is a resulting stage increase that may keep the side channels and sloughs flooded, even as the discharge reduces to low winter levels. Figures 1 and 2 depict the channel network within FA-128.

3 RIVER2D MODELING FRAMEWORK

River2D is a two-dimensional, depth-averaged, finite-element model developed by the University of Alberta and compiled to execute in Microsoft Windows (Steffler and Blackburn, 2002). It is intended for use on natural streams and rivers and has special features for accommodating supercritical /subcritical flow transitions and variable wetted area. It is functionally a transient model but provides for an accelerated convergence to steady-state conditions. The model includes a capability for specifying a floating but immobile ice cover of spatially variable extent, thickness, and roughness and determining how the additional frictional resistance of the ice cover modifies two-dimensional flow and river stage. However, this report applies only to model development and calibration for open-water conditions; ice-covered conditions will be modeled at a later date.

3.1 Hydrodynamic Equations

River2D hydrodynamics are based on the two-dimensional, depth-averaged, St. Venant equations, expressed in a mass- and energy-conservative form. Pressure distribution in the vertical coordinate is assumed to be hydrostatic; Coriolis and wind forces are assumed to be negligible; and water density is constant both in space and time. The model equations solve for three dependent variables: water depth and discharge intensities (q_x, q_y) in two respective horizontal coordinates.

Conservation of mass:

$$\frac{\partial H}{\partial t} + \frac{\partial q_x}{\partial x} + \frac{\partial q_y}{\partial y} = 0 \qquad (1)$$

Conservation of x-direction momentum:

$$\frac{\partial q_x}{\partial t}+\frac{\partial\left(Uq_x\right)}{\partial x}+\frac{\partial\left(Vq_x\right)}{\partial y}+\frac{g}{2}\frac{\partial H^2}{\partial x}=gH\left(S_{0x}-S_{fx}\right)+\frac{1}{\rho}\left(\frac{\partial H\tau_{xx}}{\partial x}+\frac{\partial H\tau_{xy}}{\partial y}\right) \tag{2}$$

Conservation of y-direction momentum:

$$\frac{\partial q_y}{\partial t}+\frac{\partial\left(Uq_y\right)}{\partial x}+\frac{\partial\left(Vq_y\right)}{\partial y}+\frac{g}{2}\frac{\partial H^2}{\partial y}=gH\left(S_{0y}-S_{fy}\right)+\frac{1}{\rho}\left(\frac{\partial H\tau_{yx}}{\partial x}+\frac{\partial H\tau_{yy}}{\partial y}\right) \tag{3}$$

where H is water depth; U and V are the depth-averaged velocities in the x and y coordinate directions, respectively; g is gravitational acceleration; S_{0x} and S_{0y} are the bed slopes in the x and y coordinate directions, respectively; S_{fx} and S_{fy} are the corresponding friction slopes; and τ_{xx}, τ_{xy}, τ_{yx}, and τ_{yy} are the components of the horizontal turbulent stress tensor. The discharge intensities are related to the horizontal velocity components by $\left(q_x,q_y\right)=H(U,V)$.

3.2 Bed Resistance

The directional components of friction slope depend on the corresponding bed shear stresses $\left(\tau_{bx},\tau_{by}\right)$, which are related to the depth-averaged velocity through a non-dimensional Chezy coefficient (C_s).

$$\left(S_{fx},S_{fy}\right)=\frac{\left(\tau_{bx},\tau_{by}\right)}{\rho gH}=\frac{(U,V)\sqrt{U^2+V^2}}{gHC_s^2} \tag{4}$$

The non-dimensional Chezy coefficient can be derived by assuming that the vertical velocity profile is logarithmic and taking a depth average from surface to bottom; yielding,

$$C_s=5.75\log\left(12\frac{H}{k_s}\right) \tag{5}$$

where k_s is the effective roughness height of the boundary at each computational node and serves as a calibration parameter for adjusting model water-surface elevations and velocities to measured data.

3.3 Turbulent Shear Stress

Depth-averaged transverse shear-stress tensor is modeled with a Boussinesq-type eddy viscosity formulation

$$\boldsymbol{\tau}=\nu_t\begin{bmatrix}\left(\frac{\partial U}{\partial x}+\frac{\partial U}{\partial x}\right) & \left(\frac{\partial U}{\partial y}+\frac{\partial V}{\partial x}\right)\\ \left(\frac{\partial V}{\partial x}+\frac{\partial U}{\partial y}\right) & \left(\frac{\partial V}{\partial y}+\frac{\partial V}{\partial y}\right)\end{bmatrix} \tag{6}$$

where the eddy viscosity coefficient (ν_t) is related to the bed shear stress by

$$\nu_t=\varepsilon H\sqrt{\frac{\left|\vec{\tau}_b\right|}{\rho}}=\varepsilon\frac{H\sqrt{U^2+V^2}}{C_s}\ . \tag{7}$$

The coefficient ε is user definable, but the default value of 0.5 was used for this modeling effort. River2D offers the option of including two additional components of the eddy viscosity coefficient; however, these components only apply under limited conditions and were deactivated by default.

3.4 Wetting and Drying

Sections of the model domain can wet or dry depending on upstream discharge, bed morphology, and bed roughness. To effect wetting and drying computationally, River2D shifts from surface-water flow equations to groundwater flow equations when the water-surface elevation at a computational node drops below the node's ground-surface elevation. Specifically, the water mass-conservation equation is replaced by a linearized, two-dimensional, groundwater equation for flow in an isotropic, homogeneous, unconfined aquifer:

$$\frac{\partial H}{\partial t} = \frac{T}{S}\left[\frac{\partial^2 (H + z_b)}{\partial x^2} + \frac{\partial^2 (H + z_b)}{\partial y^2}\right] \quad (8)$$

where T is transmissivity; S is storativity; and z_b is the ground-surface elevation. Although both T and S are user definable variables, it is the ratio T/S that controls groundwater flow. For the quasi-steady conditions modeled, surface-water flow dominated groundwater flow in the areas of interest, and alteration of the default ratio (= 0.1 m^2/d) by two orders of magnitude up or down did not greatly alter model results except slightly in some isolated topographic depressions filled solely by groundwater inflow. Note also that this equation is primarily a method of computational simplification to model regions that wet and dry; it is not intended to represent the complexity of actual groundwater flow except in a very general sense.

3.5 Computational Mesh

River2D employs a spatially variable, triangular mesh and finite-element computations. Smaller mesh size can be used to better define bathymetric changes in a wetted channel; whereas, larger mesh size can be used to model bordering upland areas that do not wet even under extreme discharge conditions. Transitions between areas of smaller and larger mesh size must be gradual to minimize numerical errors. Computational requirements generally increase for smaller, more numerous mesh elements, so mesh generation must exercise a balance between computational efficiency (i.e., a reasonable model run time) and providing sufficient spatial resolution to capture the relevant physics of fluid flow within the region of interest. The River2D modeling suite includes a basic grid generator for developing the computational mesh.

4 MODEL SETUP FOR THE SLOUGH 8A COMPLEX (FA-128)

4.1 Topography

The River2D bed topography for FA-128 was derived from a combination of high-resolution LiDAR for the upland areas and cross-channel bathymetric surveys for the wetted areas. The individual geo-referenced elevation data were overlaid by a continuous 2D GIS surface, which was digitized as a Triangulated Irregular Network (TIN) for importation into the River2D model. The resulting TIN contained more than 200,000 elevation nodes, providing exceptionally detailed topography and bathymetry for the focus area (Figure 1).

4.2 Bed Roughness Height (k_s)

Frictional resistance of the bed is controlled in River2D by the bed roughness height (k_s), which is both an initial input parameter and potentially a calibration parameter to obtain correct model response for water depth and velocity. In the simple case of a flat, spatially uniform bed with unimodal substrate size, the bed roughness height approximately describes the grain or cobble diameter of the bed material. For beds of mixed substrate sizes, the larger roughness elements can increase the substrate effective roughness considerably. For vegetated areas that wet and dry, effective bed roughness height must also include the additional frictional resistance of the vegetation.

Miller Ecological and R2 Resources conducted substrate mapping of FA-128 into descriptive habitat-substrate classes. Subsequent substrate sampling by Tetra Tech identified dominant and subdominant substrate diameters (D_{84}) and dominant and subdominant substrate fractions to develop a representative substrate size for each habitat-substrate class. Vegetation resistance was included for upland areas. FA-128 was subsequently mapped by geo-referenced subareas into 36 representative substrate sizes varying from 1 mm (silty mud) to 362 mm (vegetated upland). These size classes were aggregated by HDR to reduce the number of modeled size classes from 36 to 15, with the representative size of the aggregated classes taken as the areal-averaged mean of the original size classes. As an initial estimate in River2D, $k_s = \alpha D_{84}$, where α (=1 to 3) is a constant of proportionality (Steffler and Blackburn, 2002). Preliminary modeling found that $a = 1$ provided reasonable results for matching water-surface elevation. Minor changes to bed roughness were made based on detailed aerial photography of exposed reaches, bars, and beaches and also during model calibration. These changes had minimal effect on model results, even locally, suggesting that bed roughness height was scaled appropriately for FA-128. The final spatial distribution of modeled bed roughness height is presented in Figure 2.

4.3 Computational Mesh

Development of the spatially variable triangular mesh for FA-128 was an iterative process. An initial mesh containing approximately 10,000 nodes was developed first. Preliminary model runs and model calibration efforts helped identify areas of the model domain where finer spatial resolution was required. The final computational mesh for FA-128 contains 28,475 nodes (Figure 3).

Finer mesh size results in more computational nodes within the model domain and often also requires a shorter time step to maintain stability of the numerical approximations; therefore, mesh development typically necessitates a compromise between achieving fine spatial resolution everywhere and achieving reasonable computational efficiency. As a rough "rule of thumb," a minimum of four and preferably ten or more cells in each coordinate direction are required to accurately resolve an important feature of the flow field (Steffler and Blackburn, 2002). Achieving this degree of spatial resolution is easy for the Susitna River mainstem, which is approximately 350–750-ft wide in FA-128. However, achieving a similar degree of spatial resolution is not feasible in some of the small side sloughs of FA-128, which measure as little as 50-ft across. It is particularly difficult to achieve sufficient mesh resolution to resolve the narrow, relatively steep, embankments of these small side sloughs, as will be seen when presenting some of the calibration results. Nevertheless, a compromise was achieved in the side sloughs to provide sufficient spatial resolution

to describe flow suitably well in the slough channels while sacrificing some accuracy along the steep banks. Figure 4 presents a close-up view of mesh resolution for a section of Slough 8A.

4.4 Boundary Conditions

4.4.1 Inflow Boundary Condition

The Inflow boundary condition for all open-water calibrations was specified as the mean discharge measured during the calibration interval by the Susitna River at Gold Creek gauge (USGS 1529200).

Table 1. Calibration intervals, model parameter values, and three "goodness-of-fit" statistics

Survey Date	Discharge (cfs)	Discharge (cms)	K	T/S Ratio (m^2/d)	*RMSE* (ft)	*ME* (ft)	*ESD* (ft)
27-Jun-2013	26,132	739.971	0.46	0.1	0.22	-0.02	0.22
28-Jun-2013	28,150	797.119	0.46	0.1	0.50	0.23	0.44
02-Jul-2013	24,705	699.568	0.46	0.1	0.34	-0.06	0.34
24-Jul-2013	20,132	570.075	0.50	0.1	0.35	0.01	0.35
10-Sep-2013	26,124	739.749	0.46	0.1	0.31	-0.13	0.29

This gauge is located approximately ten river miles upstream of FA-128, and several small tributaries and possibly additional groundwater enter the Susitna River within this section. Consequently, there may be some tendency for the applied boundary condition to underestimate inflow to the model domain. However, it is expected that the error from omitting the tributary and groundwater inflow is generally small relative to flow in the Susitna River itself. As well, any attempt to estimate the upstream contribution of small tributaries and groundwater inflow is just as likely to introduce arbitrary error or bias. Thus, applying the discharge measured by the USGS gauge without modification was selected as the most candid approach.

4.4.2 Outflow Boundary Condition

A common outflow boundary condition is to clamp the water-surface to a specified elevation across the entire boundary. However, for the complex outflow boundary found at FA-128, this clamped condition often resulted in areas of abrupt and unnatural change in water-surface elevation along the boundary. Thus, for all calibration intervals, a depth-unit discharge relationship was employed of the form

$$q = K h^m \tag{9}$$

where q is unit discharge; h is the flow depth; and K and m are constants. This River2D option forces a weir-type flow through each boundary element, allowing each element to adjust to local discharge and bathymetry and allowing water-surface elevation to vary more naturally along the outflow boundary. The default value for m (= 1.6667) was used for all calibration intervals; whereas, K was varied as a calibration constant from the default value of 1.0 (Table 1).

5 CALIBRATION

5.1 Calibration to Water-Surface Elevation

Surveys of water-surface elevation were made in FA-128 by Geovera on eleven dates from June through September 2013. Five of these data sets were selected for model calibration (Table 1). Water-surface elevations were surveyed at water's edge, which makes for a challenging metric to match with a model. Bathymetry and topography generally vary more rapidly along channel banks, which tends to increase errors in model bed elevation locally due to spatial averaging of the bed-elevation TIN, as well as additional spatial averaging inherent in the model's computational mesh. Thus, model response tends to be least accurate along channel edges.

Dates and setup conditions for each model calibration are summarized in Table 1, which also includes three statistical measures for model "goodness of fit" to observed data; namely, root-mean-square error (*RMSE*), mean error, (*ME*), and error standard deviation (*ESD*):

$$RMSE = \sqrt{\frac{\sum_{i=1}^{n}\left(x_{\text{modeled},i} - x_{\text{observed},i}\right)^2}{n}} \tag{10}$$

$$ME = \frac{\sum_{i=1}^{n}\left(x_{\text{modeled},i} - x_{\text{observed},i}\right)}{n} \tag{11}$$

$$ESD = \sqrt{\frac{\sum_{i=1}^{n}\left[\left(x_{\text{modeled},i} - x_{\text{observed},i}\right) - ME\right]^2}{n-1}} \tag{12}$$

where x_{observed} represents the surveyed surface-water elevation at water's edge; x_{modeled} represents the modeled surface-water elevation at the survey location, and n represents the total number of observed-versus-modeled data pairs. *RMSE* quantifies the magnitude of disagreement between observed and modeled pairs; *ME* quantifies the positive or negative bias of model results to observed data; and *ESD* provides a measure of variability of the difference between model results and observed data.

Calibration actions included adjustment of constant K in Equation (9) and refinement of the computational mesh to better resolve river flow and to improve model agreement with observed elevation data. Each calibration interval was considered acceptably calibrated when the *RMSE* was less than or equal to 0.50 ft at water's edge. Calibration results for water surface elevation are presented graphically in Figure 5 through Figure 9, which also show the locations of the measured water-surface elevations for each survey date.

5.2 Calibration to Current Speed

In addition to surveys of water-surface elevation, cross-channel transects of current speed were measured in FA-128 on two dates (2 Jul 2013, 10 Sep 2013) using a boat-mounted acoustic Doppler current profiler (ADCP). Figure 10 and Figure 11 show actual boat tracks during the velocity transects on 2 Jul 2013 and 10 Sep 2013, respectively. Each transect represents multiple passes across the channels.

Comparison of model current speeds with results from the ADCP surveys are presented and discussed below. The following points are relevant to assessing these model-data comparisons:

- Boat tracks are not linear and track positions vary slightly upstream and downstream with each crossing of a channel.
- In contrast, model transects interpolate current speed along a straight line between right- and left-bank endpoints.
- Bank endpoints were selected to position the linear model transects approximately along the average position of the multiple boat tracks across each channel.
- In several instances, model channel positions appear to be offset from channel positions indicated by the ADCP transects. For these cases, corrective offsets were added to the ADCP transect positions, and the amount of applied offset is shown on the graphical model-data comparisons. In all cases, the apparent offsets represent less than 10 percent of channel width. Potential causes of these offsets are discussed below.

5.2.1 Current-Speed Transects for 2 July 2013

Current speeds were measured on 2 July 2013 by boat-mounted ADCP along 17 cross-channel transects (Figure 10), and graphical model-data comparisons are presented in Figure 12 through Figure 16. In general, modeled current speeds compare quite well with measured speeds, although some model-data disagreements do occur. As noted previously, model accuracy suffers to some degree along the margins of steep, narrow, embankments due to the limitations of grid resolution. Bear in mind, however, that the accuracy of ADCP speed measurements also suffers along the margins of steep, narrow, embankments, so the disagreement between model and data values should not all be attributed to the model.

For cross-channel transects T1A, T2A, and T3B (Figure 12 and Figure 13), the model-data comparisons suggest that the modeled channels are offset horizontally from the position indicated by the ADCP surveys. There are several reasons why this might occur:

- Measurement offsets might occur during initial bathymetric/topographic data collection.
- Spatial-interpolation offsets might occur during development of the high-resolution TIN, when integrating LiDAR topography and discrete cross-channel bathymetric surveys.
- Spatial interpolation offsets might occur in the model computation grid due to limitations of grid resolution along steep, narrow, channel margins.
- Measurement offsets might occur during the ADCP surveys. As a case in point, cross-channel transect T4B (Figure 14) shows an approximately 15-ft horizontal offset in the measured data between successive crossings of the channel.
- Channel morphology itself might have changed between the date of the first ADCP survey and the date of the initial bathymetry surveys and collection of LiDAR-based topography. Field observations in FA-128 over several years have confirmed that channel morphology can be highly dynamic.

In all instances, the apparent offset between modeled and measured channel positions represents less than 10 percent of the channel width. Moreover, the model's characterization of channel currents for

these transects agrees quite well with the ADCP measurements, despite the apparent offset in channel positions.

Measured current speeds along cross-channel transects T2B (Figure 12) and T4C (Figure 14) show distinct two-channel morphologies; whereas, the modeled current speeds indicate a single-channel. Examination of the high-resolution TIN confirms that the modeled bathymetry represents a single channel at both transect locations. Note, however, that data collected along transect T2B for the ADCP survey on 10 Septembers 2013 (Figure 17) agrees with the single-channel morphology represented in model. Thus, model-data differences in this case might well reflect the dynamic evolution of channel morphology.

Cross-channel transect T5 presents an converse condition wherein the model results indicate a two-channel morphology, but measured data from the ADCP survey do not. Examination of the model's high-resolution TIN shows a bar extending through transect T5 from the upstream island (Figure 10). While this is a likely location for such a bar, its presence cannot be confirmed. Measured data at transect T5 for the ADCP survey on 10 Septembers 2013 (Figure 20) also suggest that a bar was not present on that date.

At cross-channel transect T6, the model over-predicts current speed substantially (Figure 15). Transect T6 is located at the confluence of a small side channel with the Susitna River mainstem (Figure 10), so a relatively small discrepancy in model bathymetry at this location could result in a relatively large difference in flow into the side channel. However, field observations at FA-128 have also demonstrated that channel morphology at the confluence of these small side channels with the mainstem is particularly dynamic, often due to winter ice scour or local flooding due to formation of ice jams downstream of the focus area. Thus, the model bathymetry along Transect T6 might not be in error, *per se*; it simply represents channel morphology at an earlier date. Note that the model speed prediction at Transect T6 more closely matches the ADCP data collected on 10 September 2013 (Figure 20), although the model still over-predicts the measured data.

5.2.2 Current-Speed Transects for 10 September 2013

Current speeds were measured on 10 September 2013 by boat-mounted ADCP along 15 cross-channel transects (Figure 11), and graphical model-data comparisons are presented in Figure 17 through Figure 20. Model-data comparisons on this date were similar to those from the previous ADCP surveys on 2 Jul 2013; in general, model results compare quite well with measured current speeds, although some model-data disagreements do occur.

For cross-channel transects T1A, T2A, and T3B (Figure 17 and Figure 18), the model-data comparisons suggest again that the modeled channels are offset horizontally from the position indicated by the ADCP surveys; however, the apparent offsets are slightly smaller on this date for transects T2A and T3B.

In contrast to the ADCP survey on 2 July 2013, ADCP speed data for transect T2B (Figure 17) does not indicate a two-channel morphology on 10 September 2013, and modeled speed agrees reasonably well with data. ADCP data along transect T4C (Figure 19) still indicates a two-channel morphology, which the model does not. Conversely, ADCP data along transect T5 still indicates a

single-channel morphology; whereas, the model speed transect is split by a bar extending through the transect from an upstream island (Figure 11).

The model again over-predicts current speeds along transect T6 (Figure 20), but model results are notably closer to measured speeds on this date.

6 SUMMARY

A River2D open-water model was developed for the Slough 8A Complex (FA-128). A high-resolution Triangulated Irregular Network (TIN) was developed by integrating high-resolution LiDAR topography with discrete cross-channel bathymetric surveys. Bed roughness was assigned using bed grain size estimated from aerial photography, LiDAR data, and direct observation at discrete locations. Vegetation roughness was included for upland areas of the model domain. A spatially variable triangular computation mesh was developed and modified iteratively to improve model performance versus measured data.

Calibration efforts included running the model for five dates from June through September 2013 for which water-surface elevations were measured at water's edge at a combined total of 305 survey locations. In addition to the water-surface data, current-speed measurements were collected by boat-mounted ADCP on two dates along 15-17 cross-channel transects. In general, model water-surface elevation and current-speed predictions agreed quite well with measured data. The River2D open-water model can suitably characterize flow through the Slough 8A Complex (FA-128) and will serve as a suitable modeling platform for future investigations of ice-cover effects during the winter.

7 LITERATURE CITED

Steffler, P., Blackburn, J., 2002. River2D, Two-Dimensional Depth Averaged Model of River Hydrodynamics and Fish Habitat. Introduction to Depth Averaged Modeling and User's Manual. University of Alberta, Edmonton, Alberta, Canada, Edmonton, Alberta, Canada, p. 41.

8 FIGURES

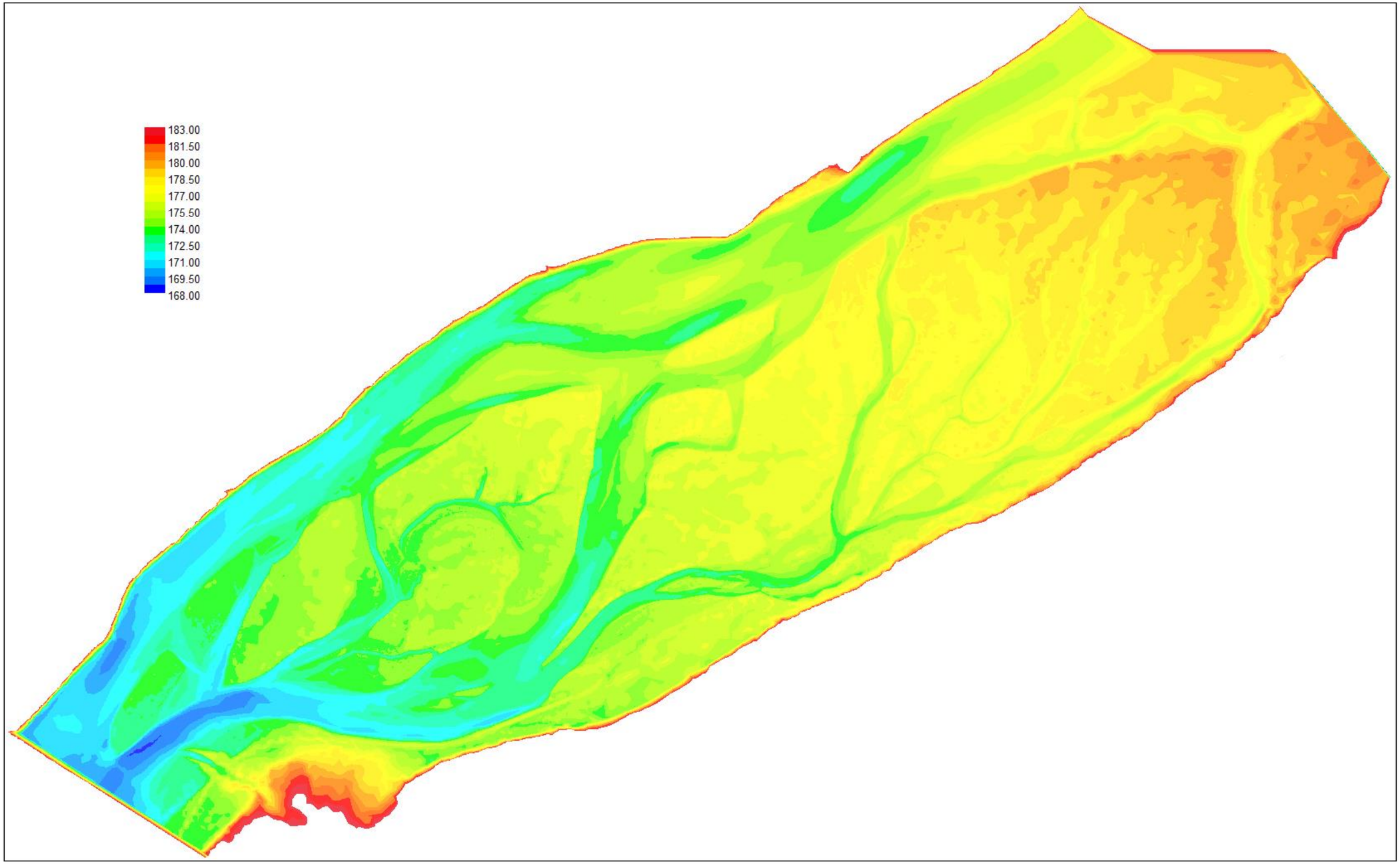

Figure 1. Slough 8A Complex (FA-128) topography and bathymetry (elevation in meters)

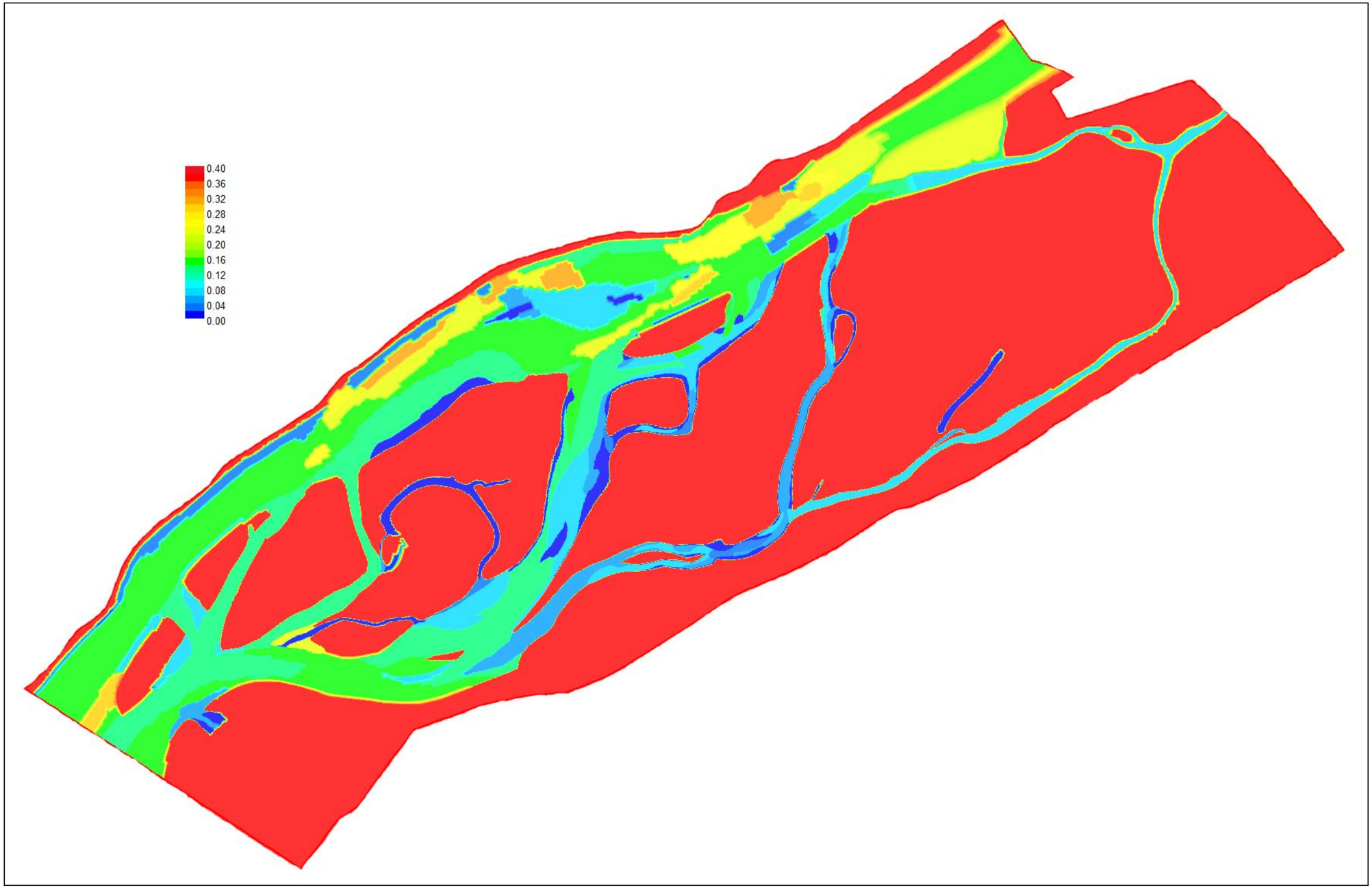

Figure 2. Slough 8A Complex (FA-128) River2D bed roughness (in meters)

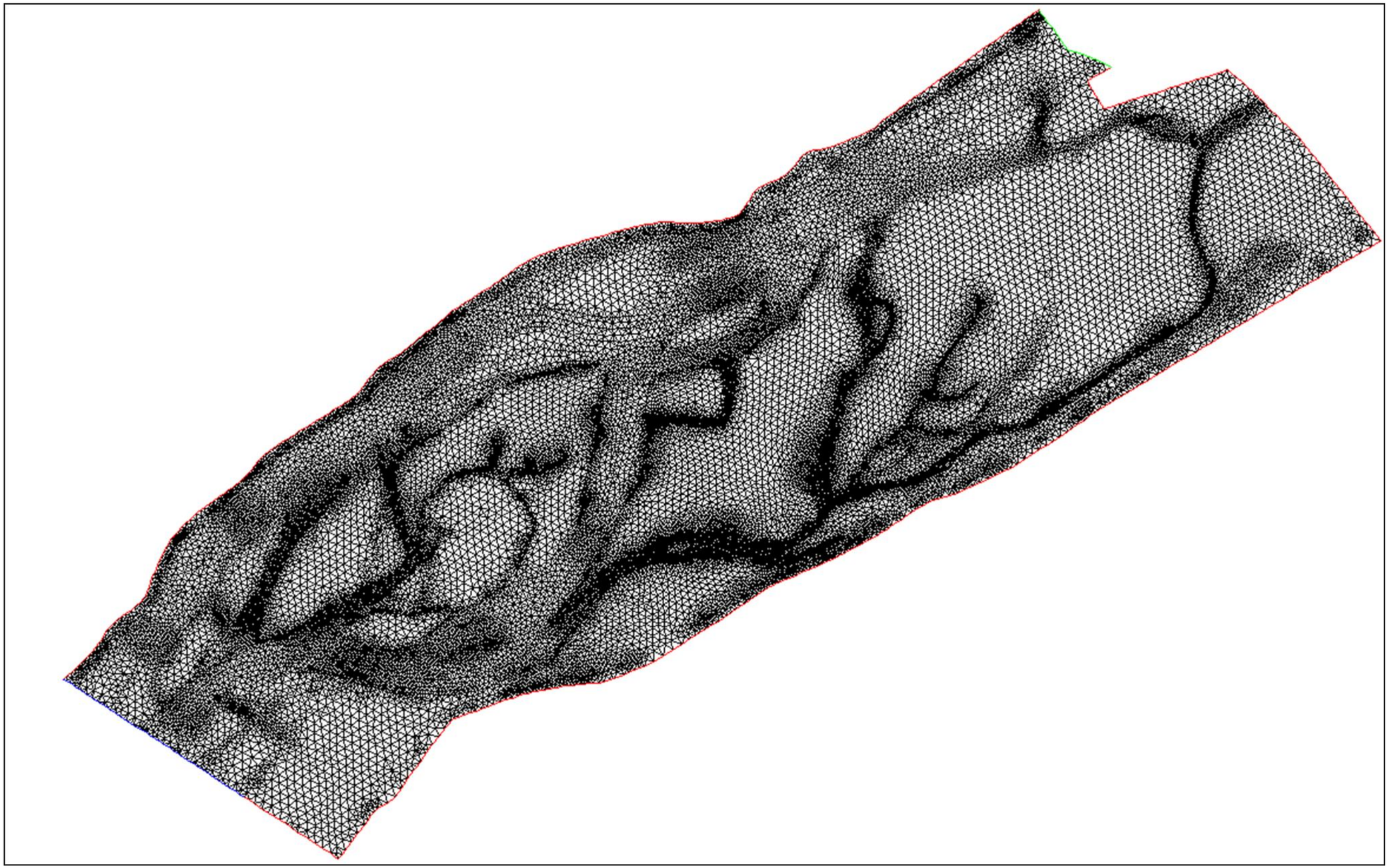

Figure 3. Slough 8A Complex (FA-128) River2D computational mesh

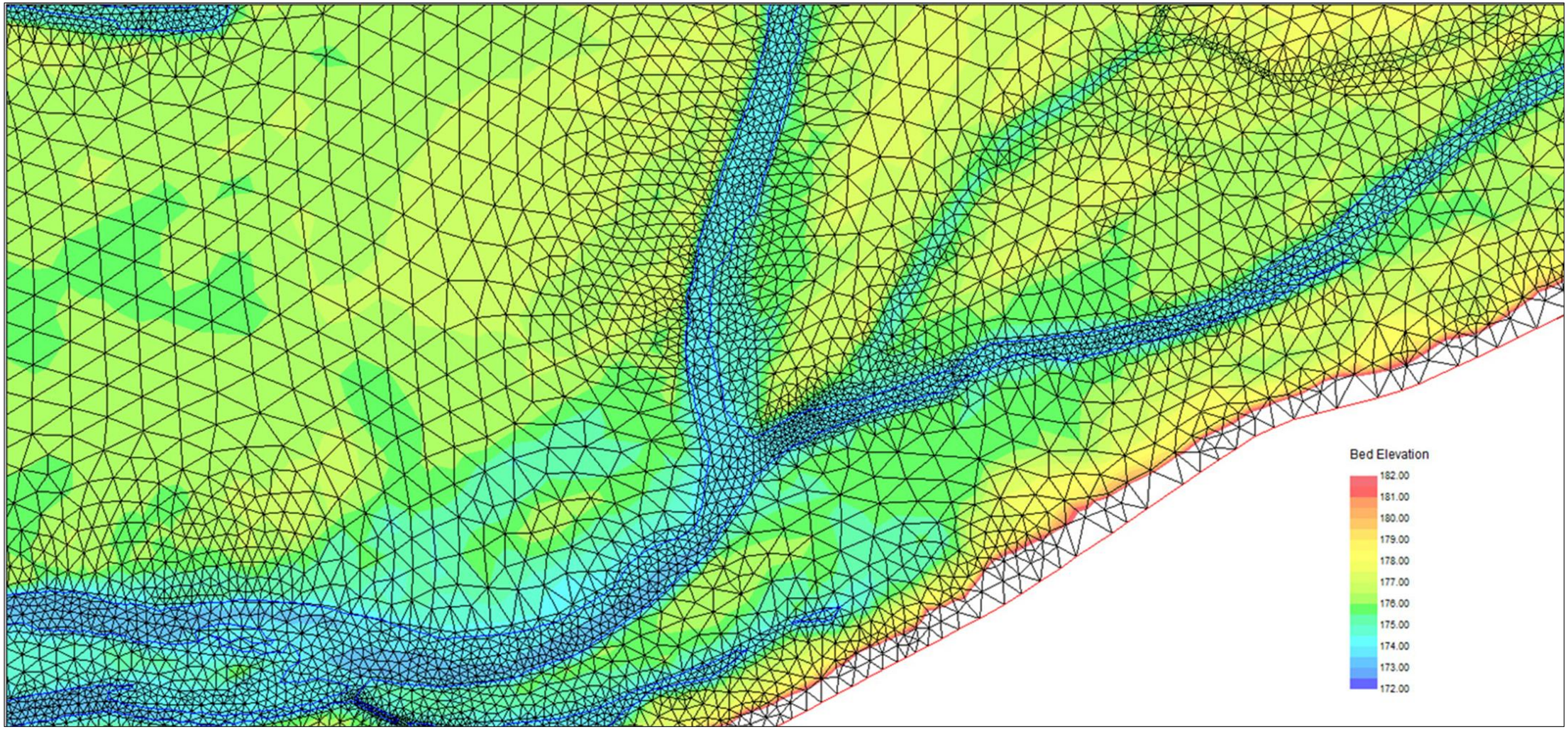

Figure 4. Slough 8A Complex (FA-128) River2D computational mesh at the confluence of several side channels with Slough 8A. (Bed Elevation in meters)

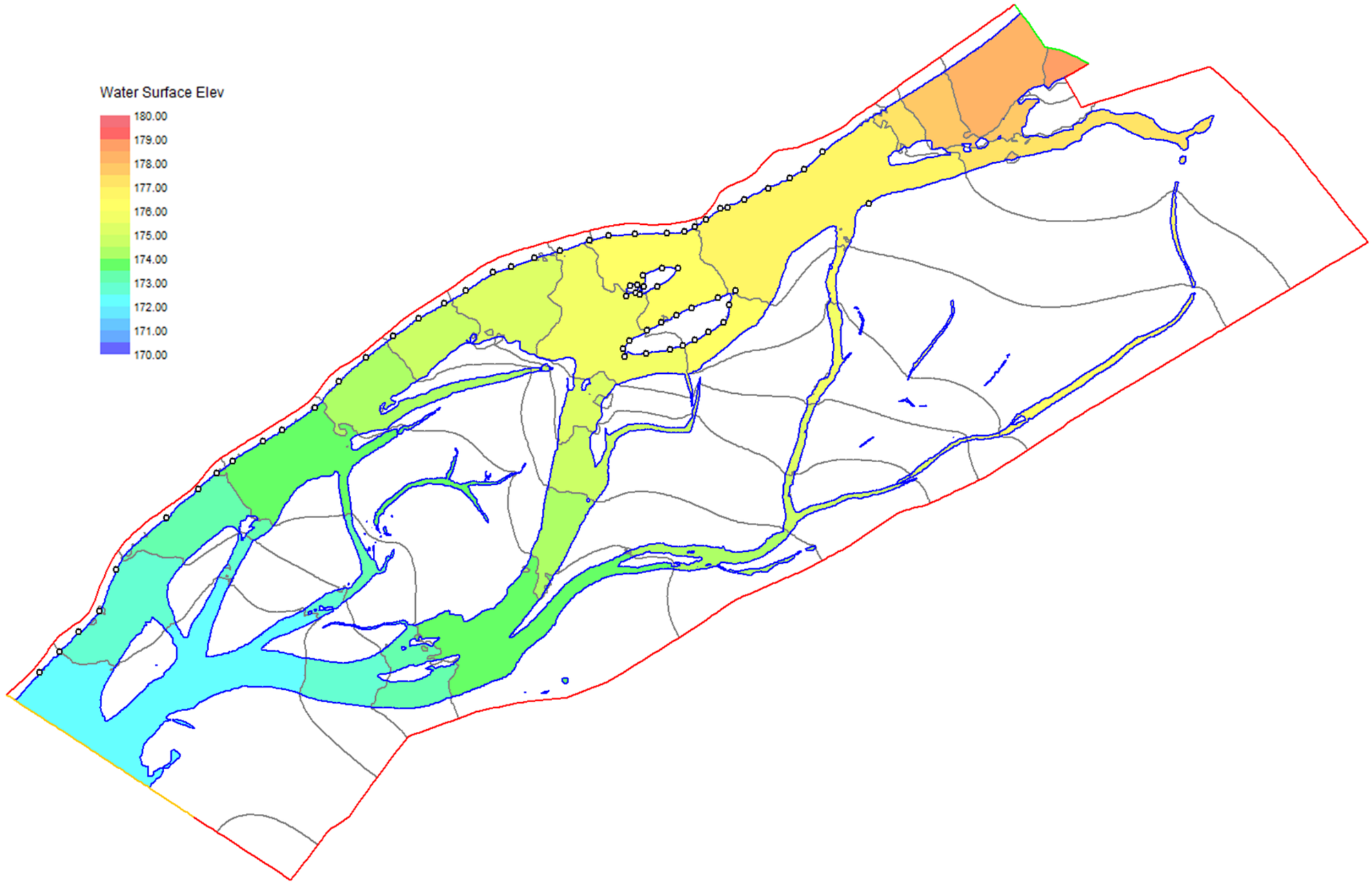

Figure 5. Slough 8A Complex (FA-128) River2D surface-water elevation (in meters) and water-edge survey locations (open circles) for the June 27, 2013 calibration. Grey contour lines are in 0.5-meter increments

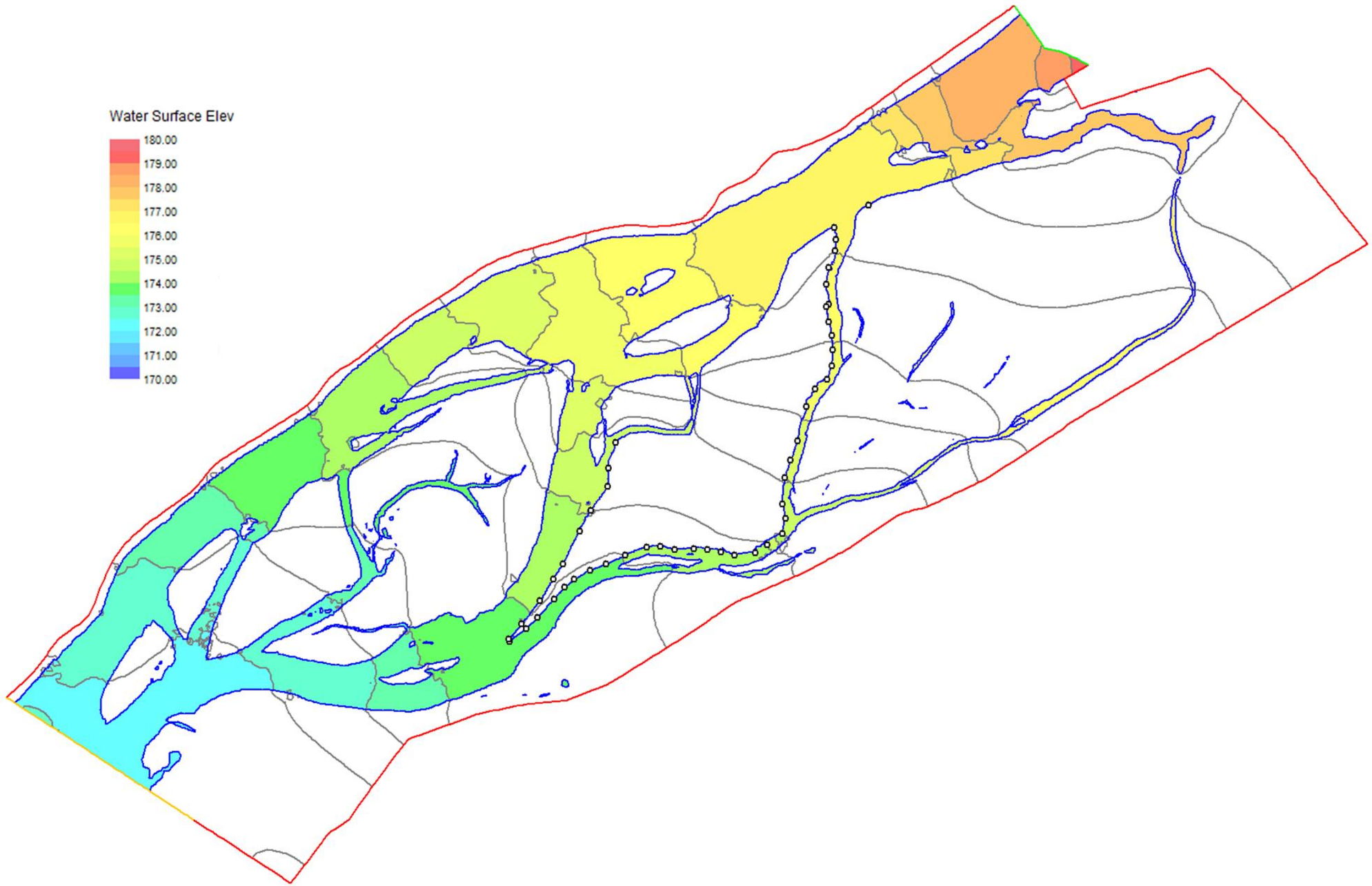

Figure 6. Slough 8A Complex (FA-128) River2D surface-water elevation (in meters) and water-edge survey locations (open circles) for the June 28, 2013 calibration. Grey contour lines are in 0.5-meter increments

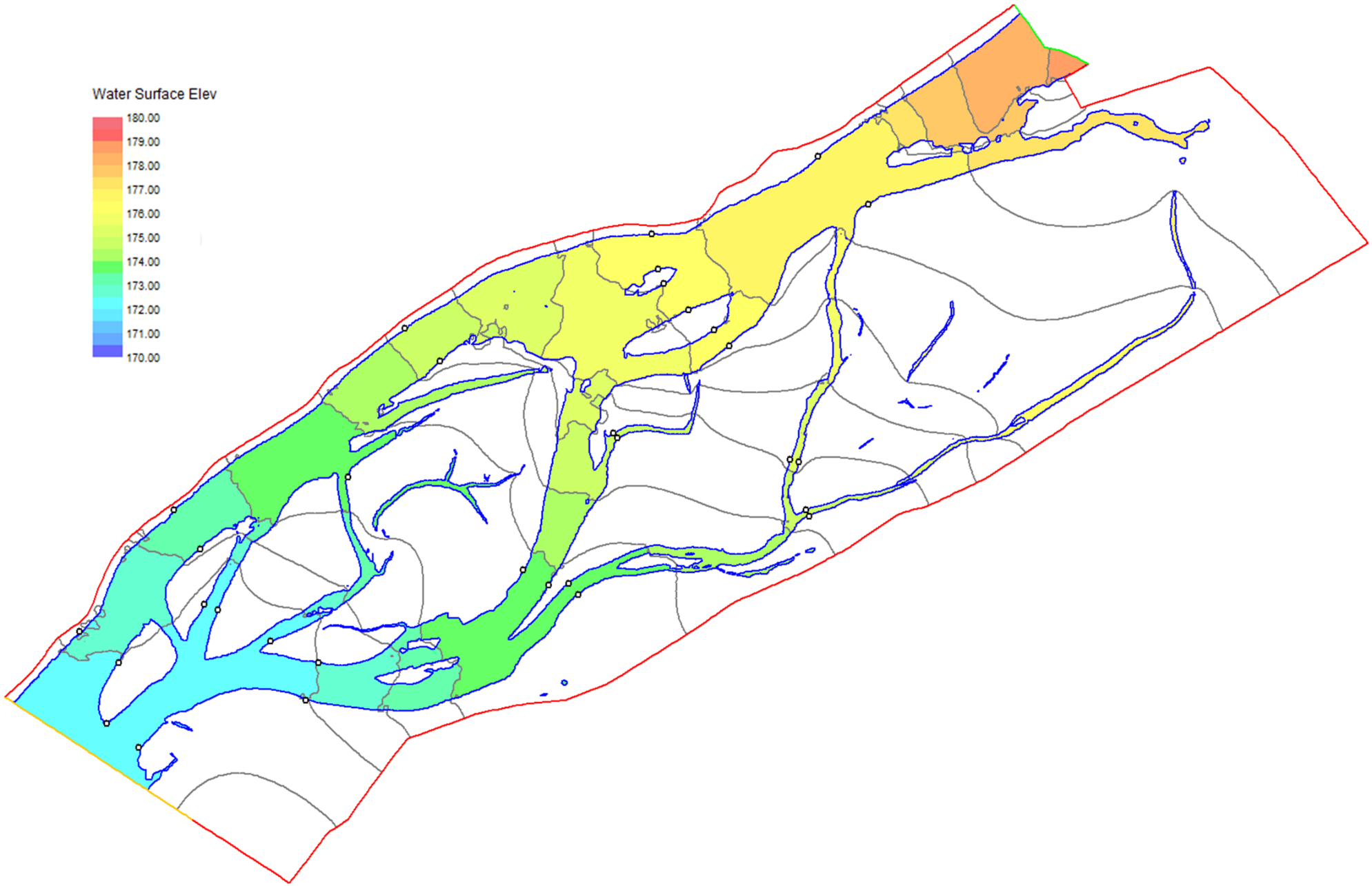

Figure 7. Slough 8A Complex (FA-128) River2D surface-water elevation (in meters) and water-edge survey locations (open circles) for the July 2, 2013 calibration. Grey contour lines are in 0.5-meter increments

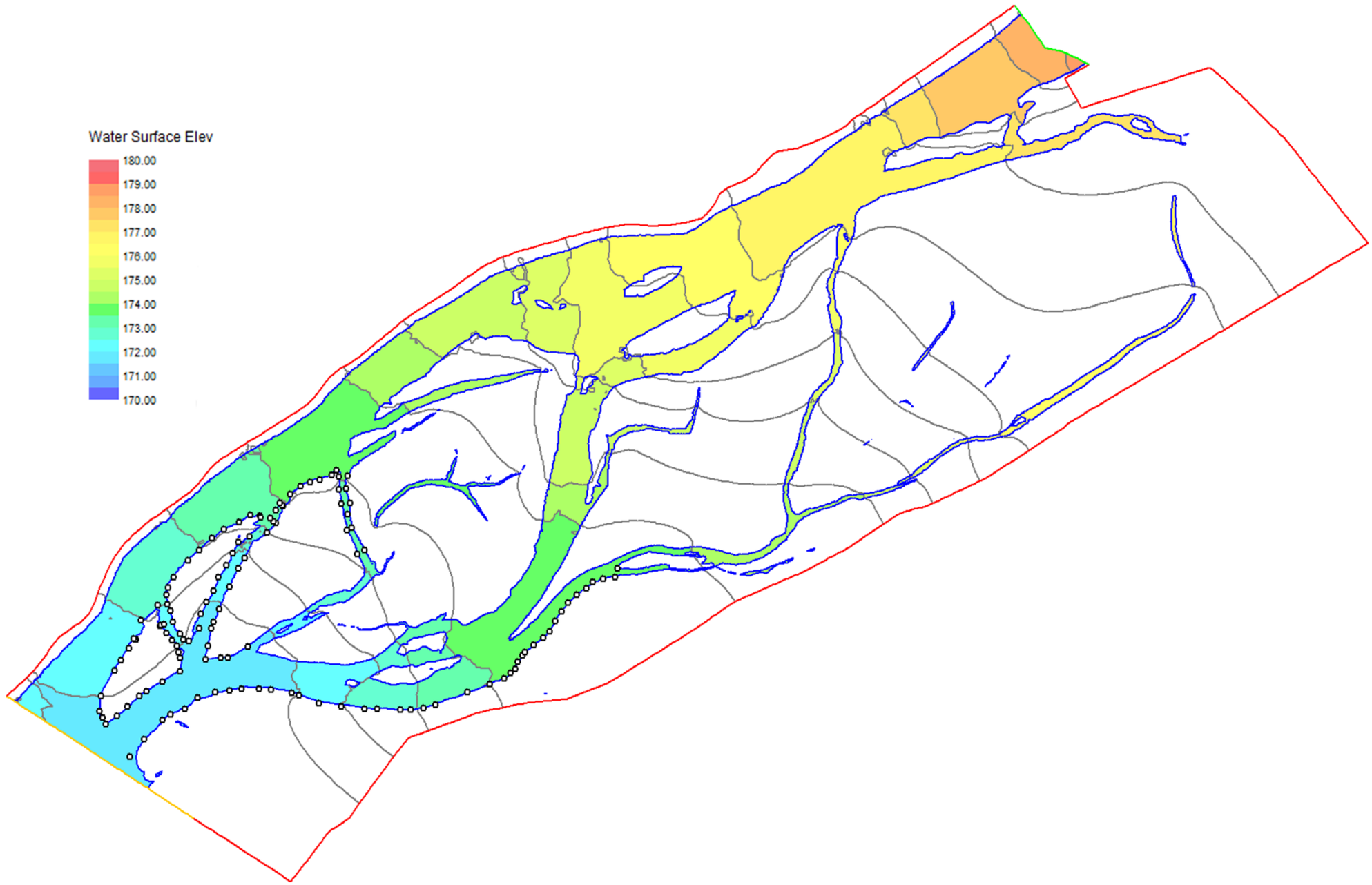

Figure 8. Slough 8A Complex (FA-128) River2D surface-water elevation (in meters) and water-edge survey locations (open circles) for the July 24, 2013 calibration. Grey contour lines are in 0.5-meter increments

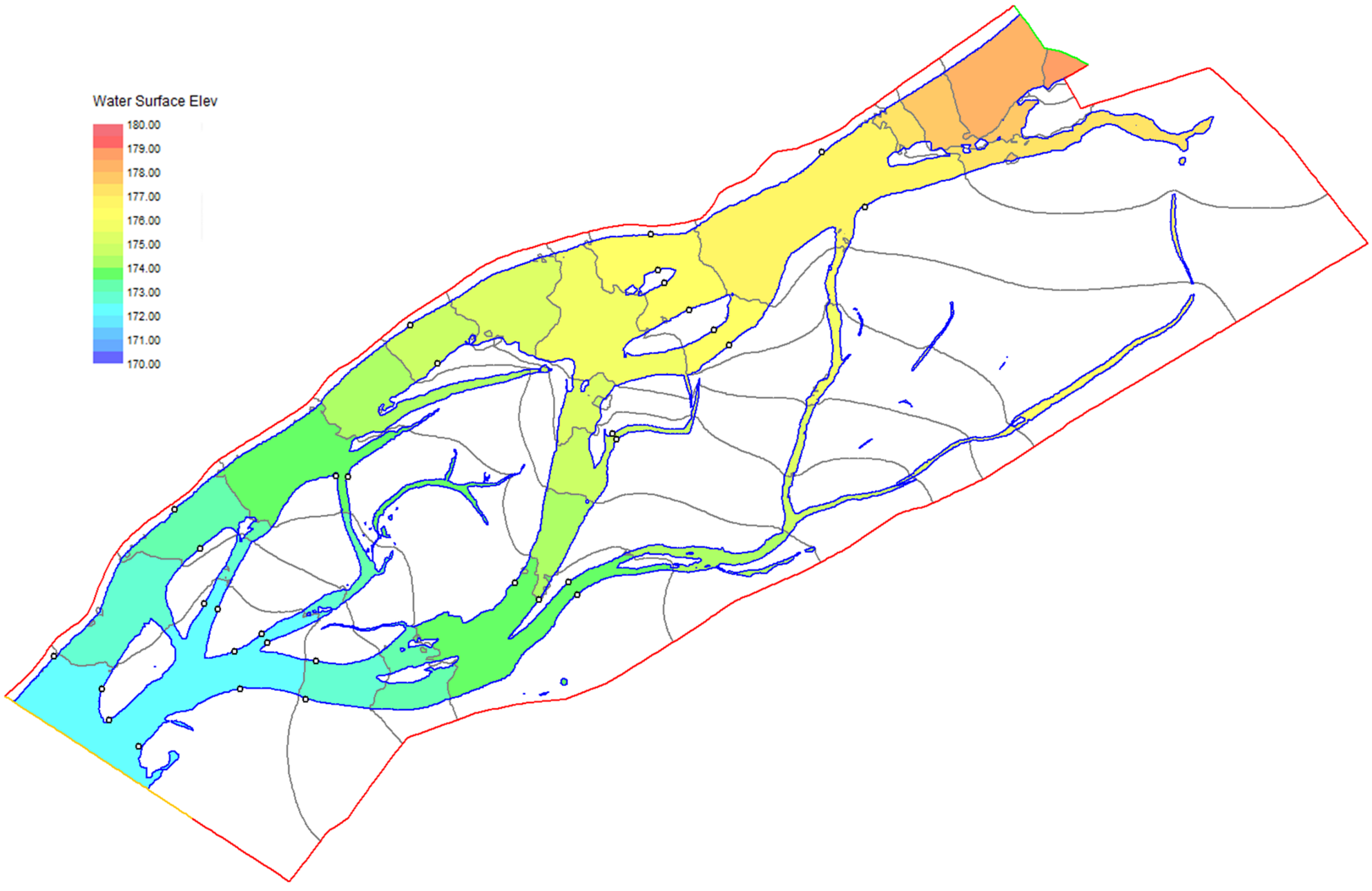

Figure 9. Slough 8A Complex (FA-128) River2D surface-water elevation (in meters) and water-edge survey locations (open circles) for the September 10, 2013 calibration. Grey contour lines are in 0.5-meter increments

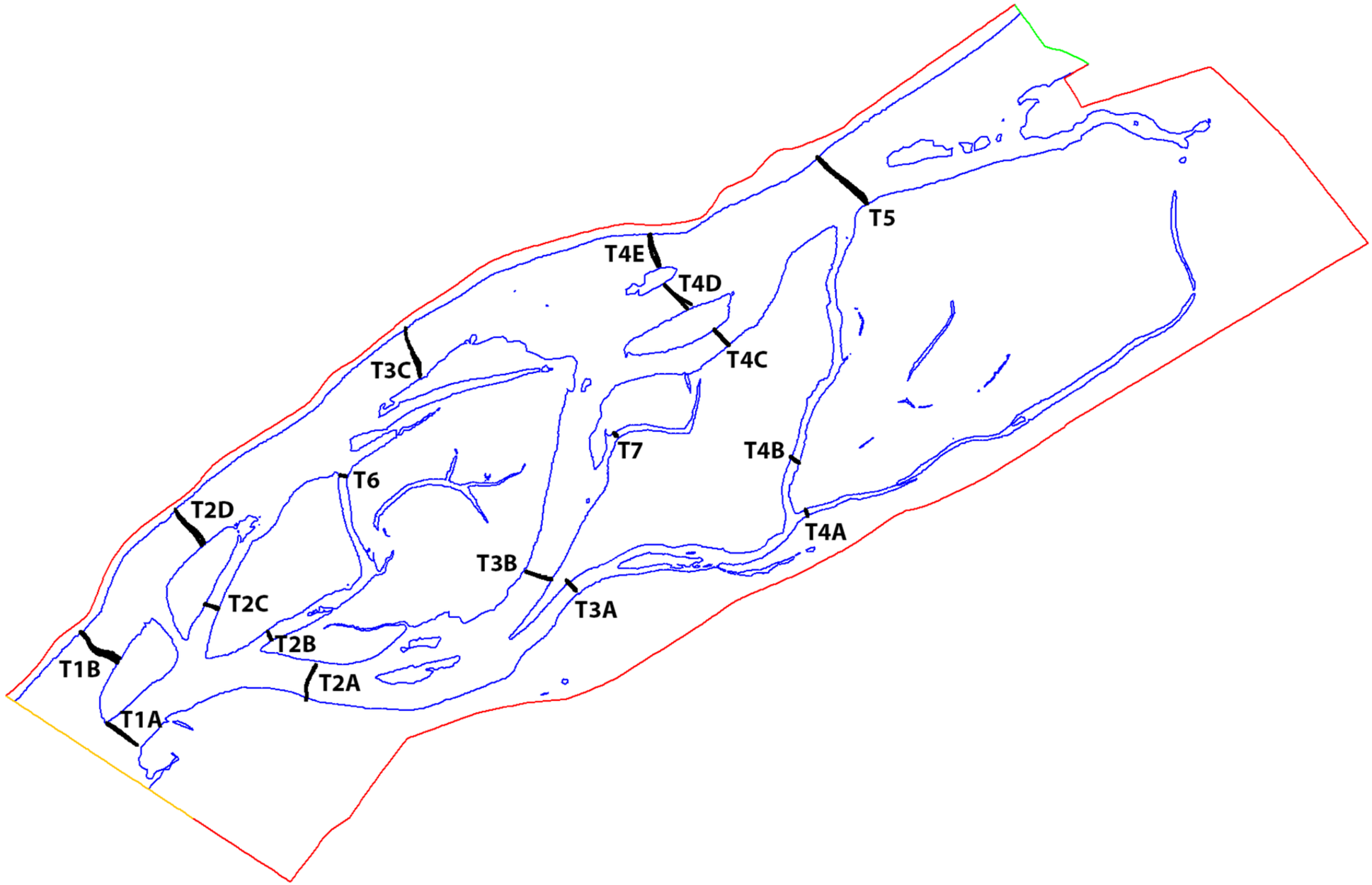

Figure 10. Slough 8A Complex (FA-128) Cross-channel velocity transects measured by boat-mounted ADCP at 17 locations on July 2, 2013

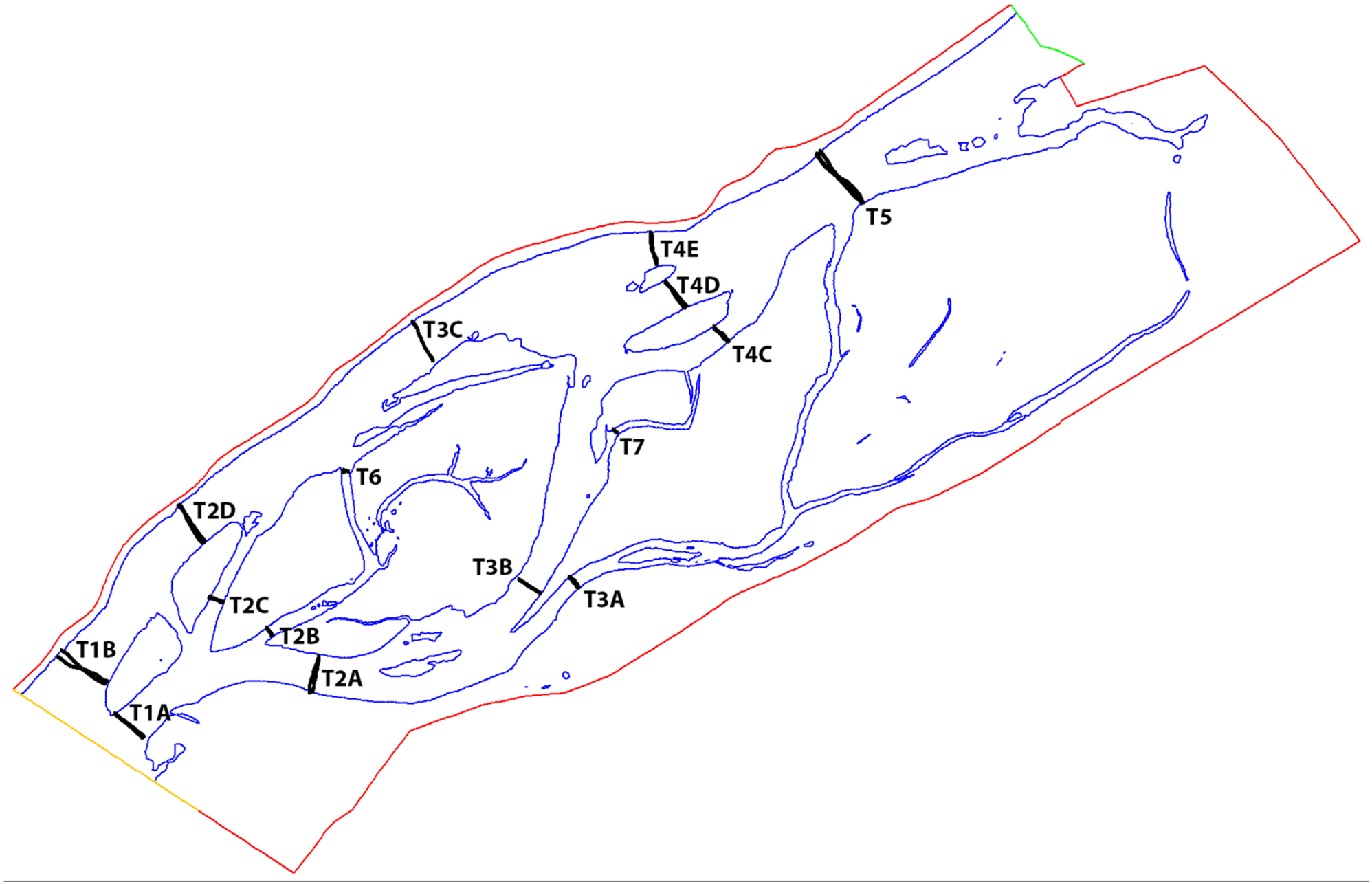

Figure 11. Slough 8A Complex (FA-128) Cross-channel velocity transects measured by boat-mounted ADCP at 15 locations September 10, 2013

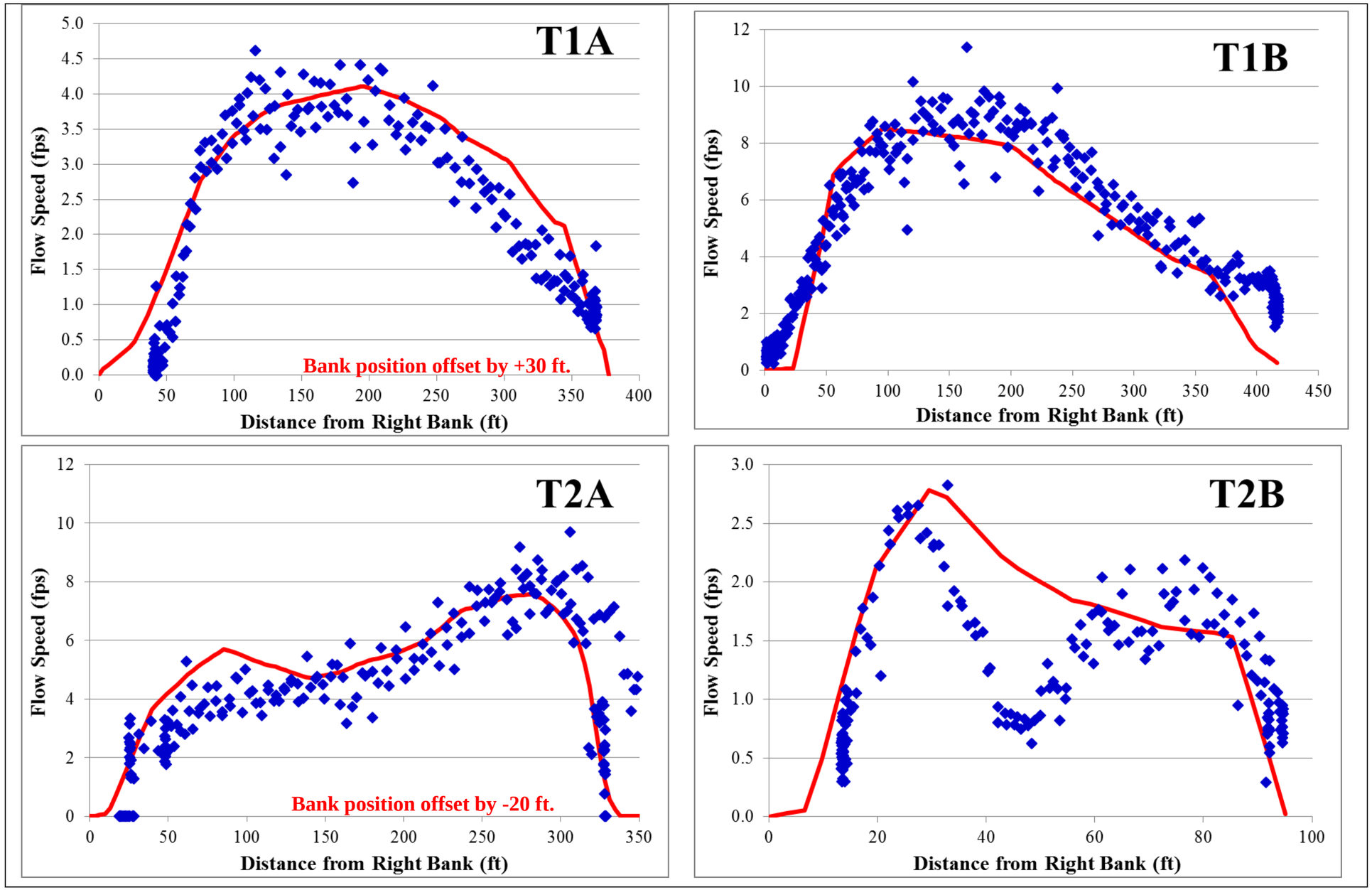

Figure 12. Slough 8A Complex (FA-128) Cross-channel velocity transects measured by boat-mounted ADCP on July 2, 2013. Red line is model transect.

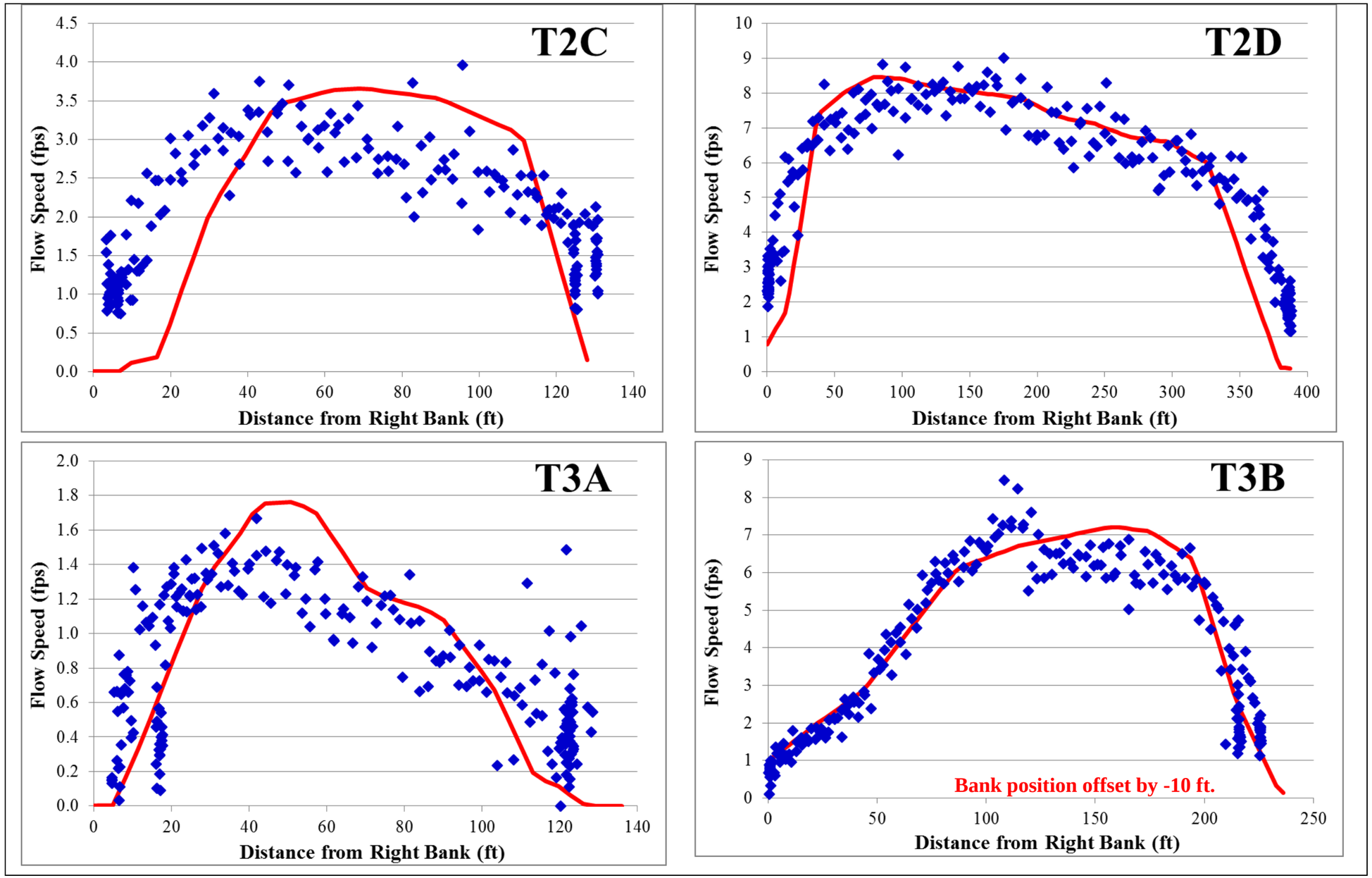

Figure 13. Slough 8A Complex (FA-128) Cross-channel velocity transects measured by boat-mounted ADCP on July 2, 2013. Red line is model transect

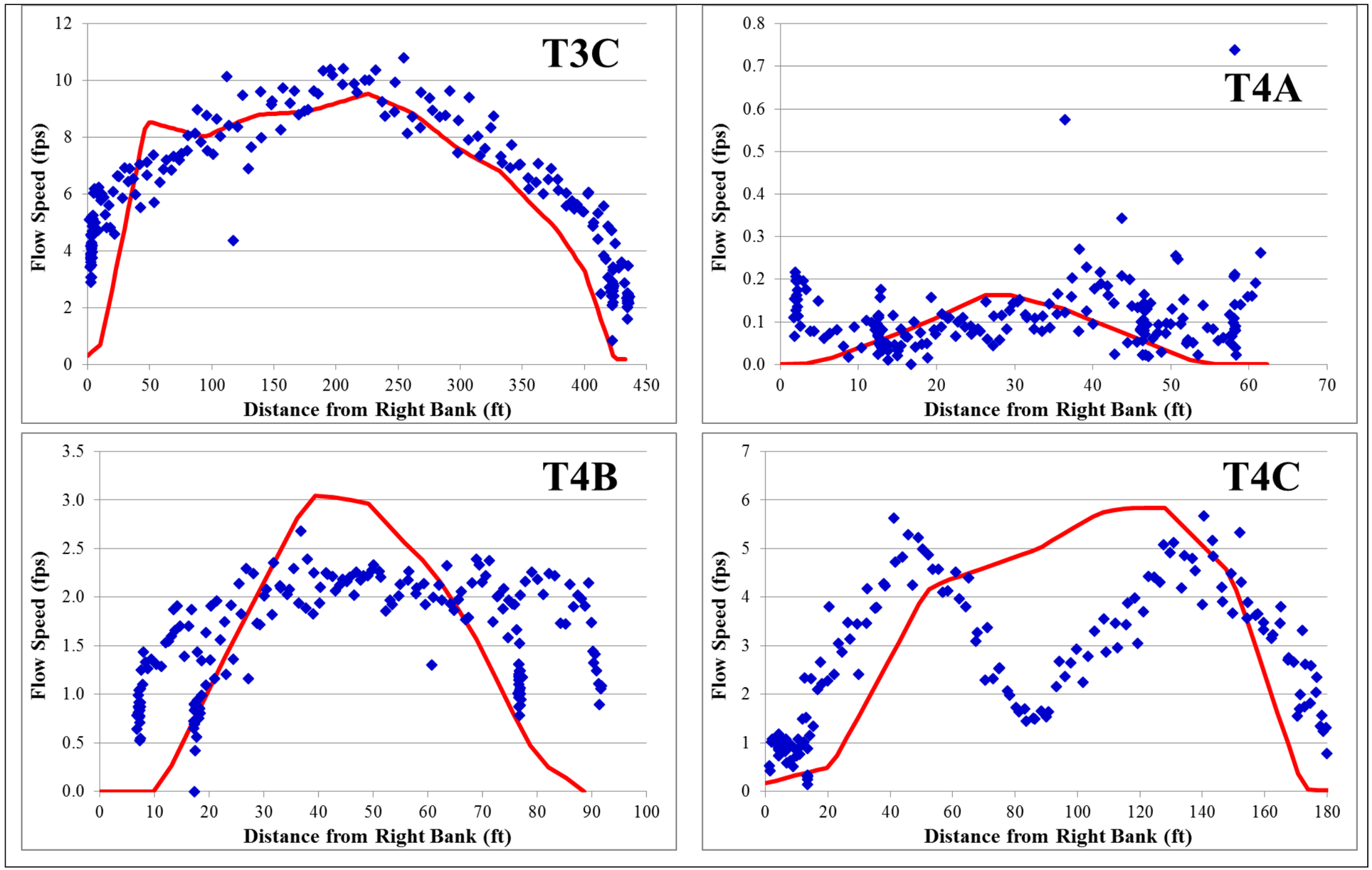

Figure 14. Slough 8A Complex (FA-128) Cross-channel velocity transects measured by boat-mounted ADCP on July 2, 2013. Red line is model transect

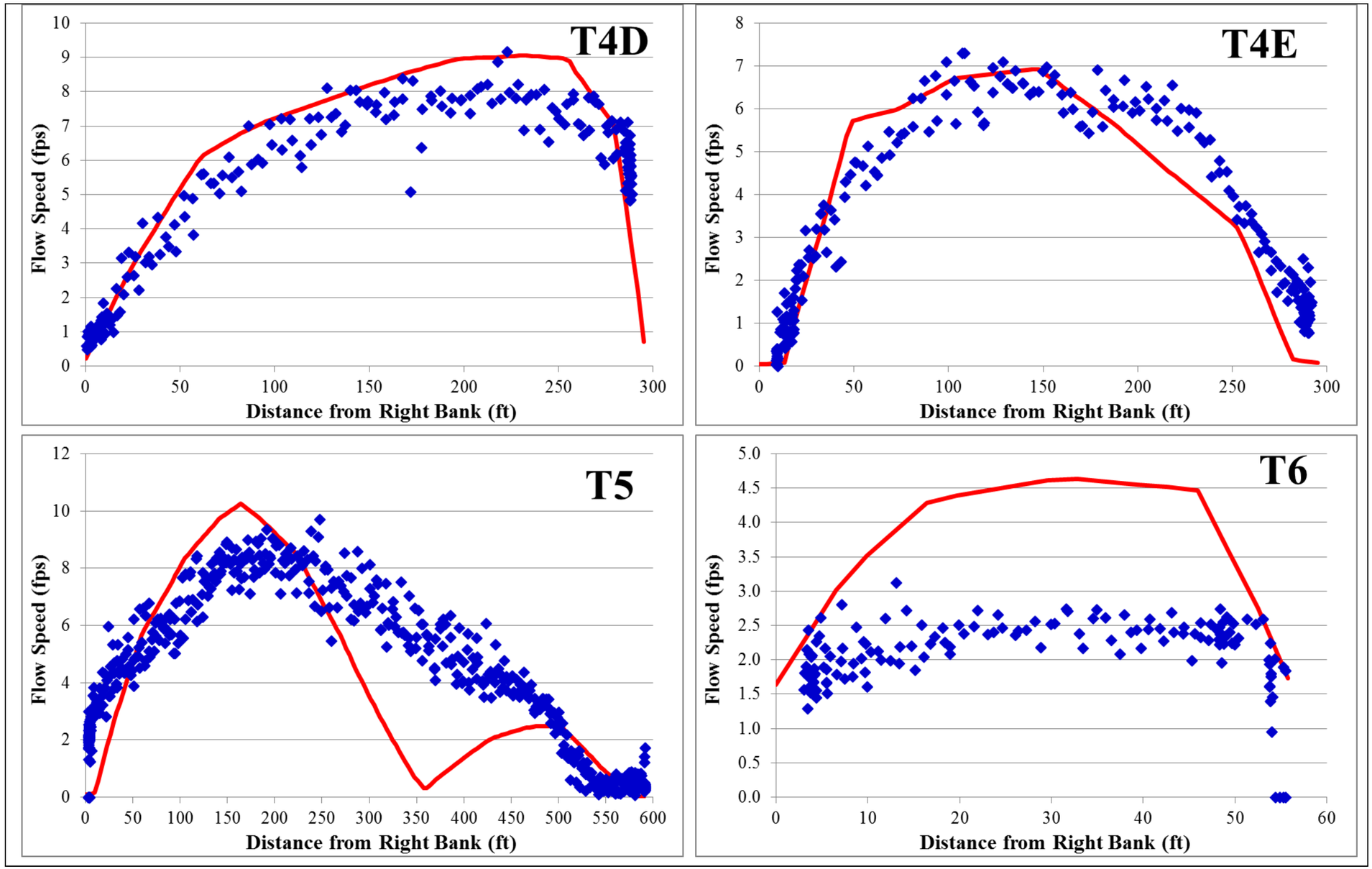

Figure 15. Slough 8A Complex (FA-128) Cross-channel velocity transects measured by boat-mounted ADCP on July 2, 2013. Red line is model transect

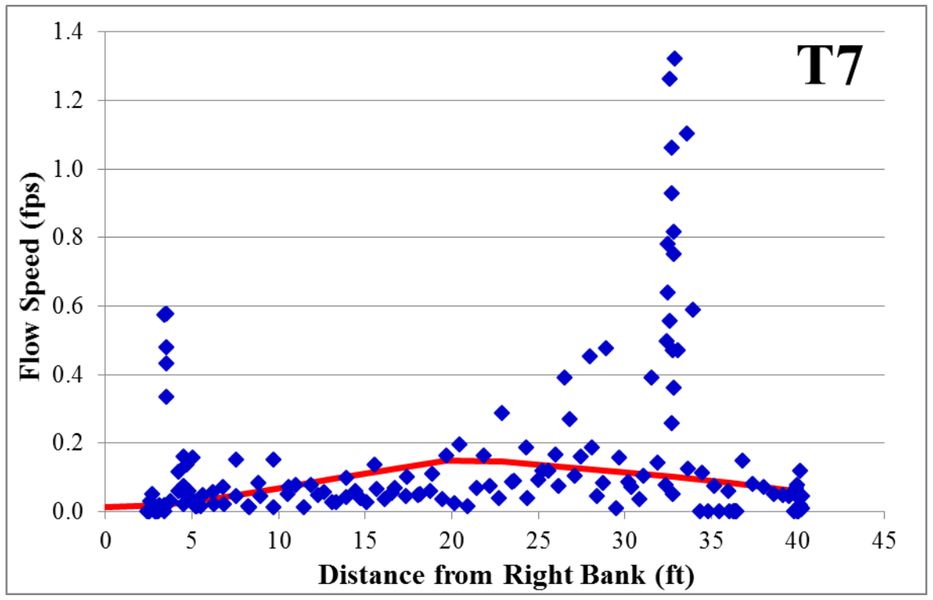

Figure 16. Slough 8A Complex (FA-128) Cross-channel velocity transects measured by boat-mounted ADCP on July 2, 2013. Red line is model transect

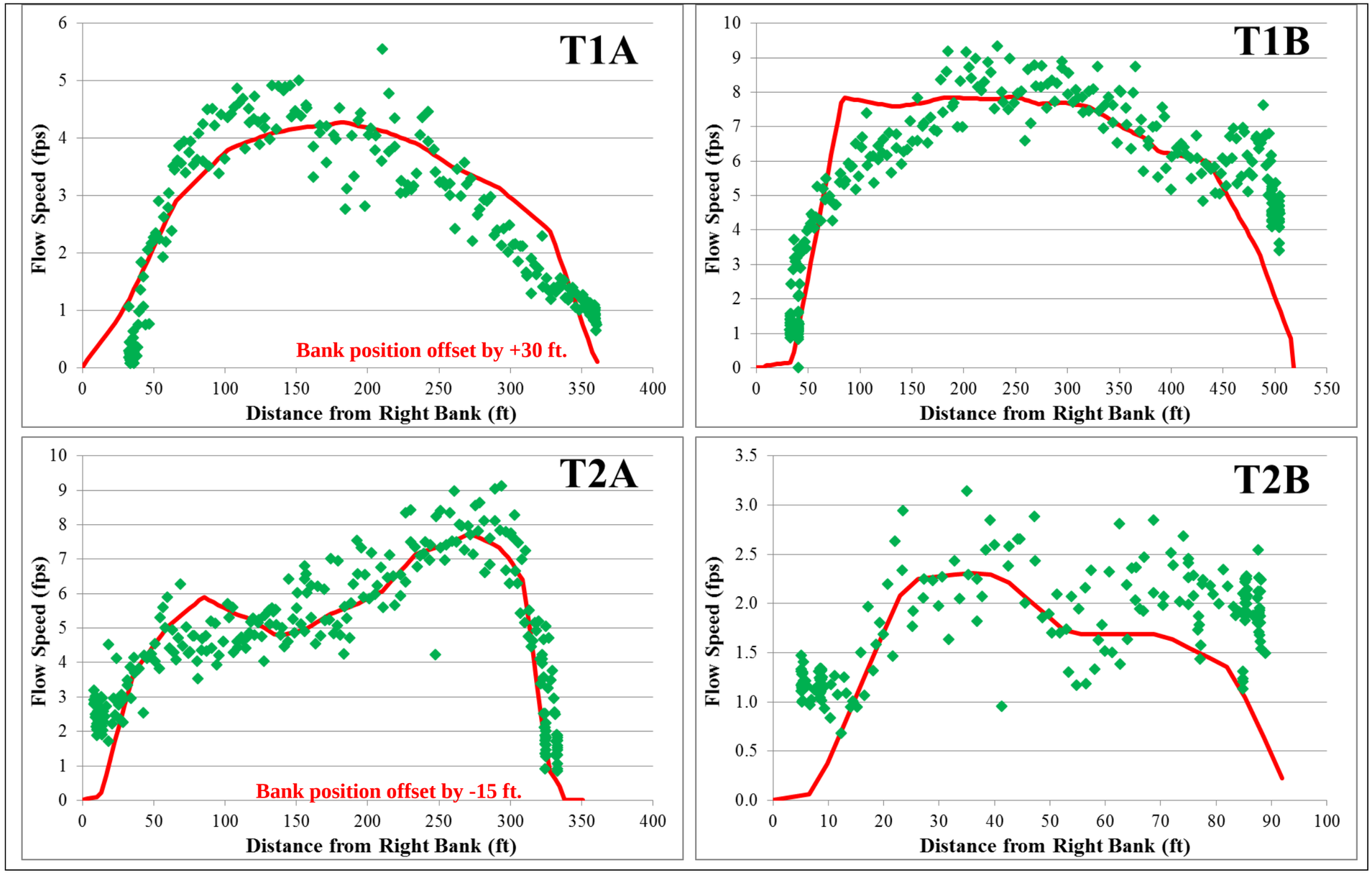

Figure 17. Slough 8A Complex (FA-128) Cross-channel velocity transects measured by boat-mounted ADCP on September 10, 2013. Red line is model transect

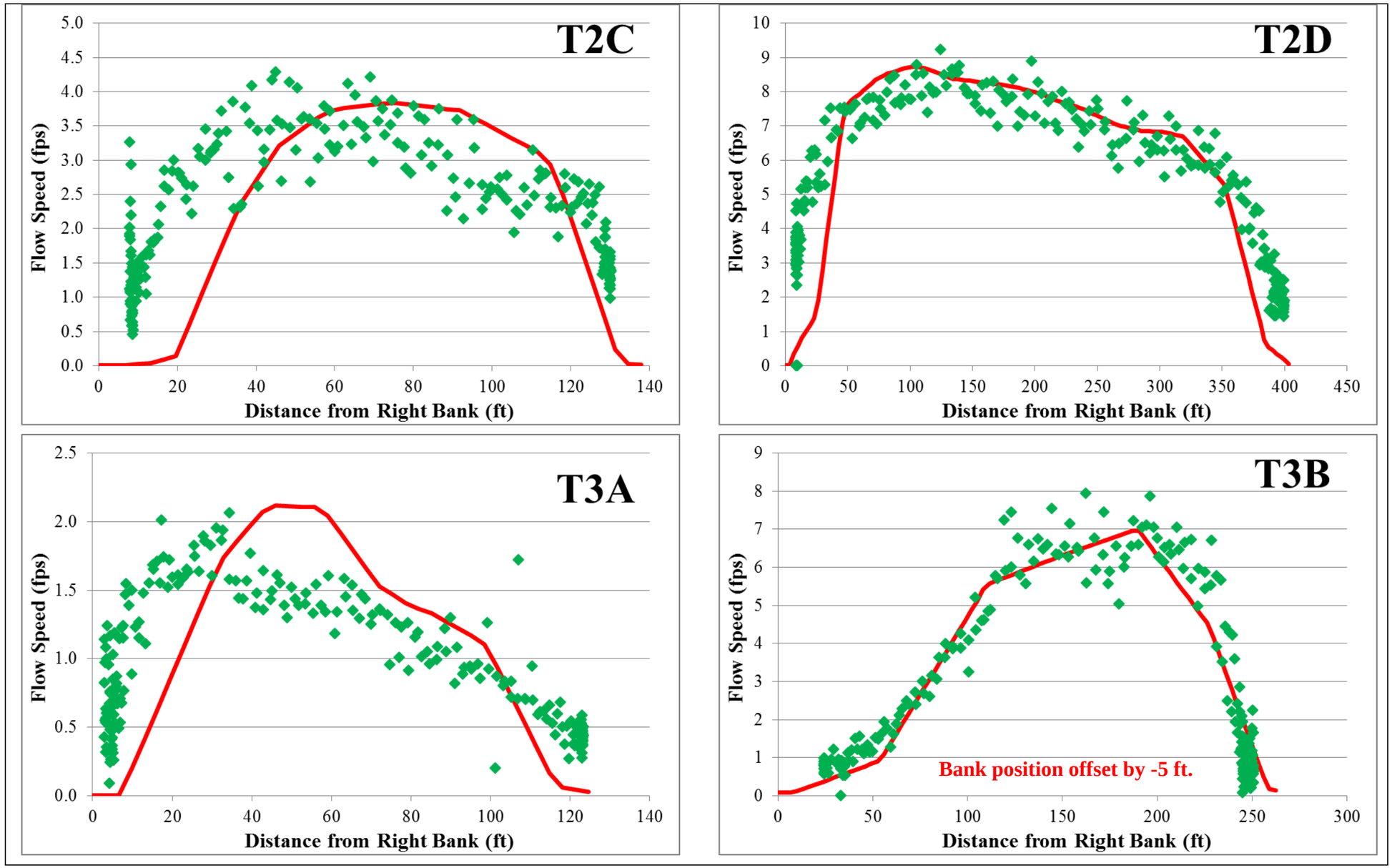

Figure 18. Slough 8A Complex (FA-128) Cross-channel velocity transects measured by boat-mounted ADCP on September 10, 2013. Red line is model transect

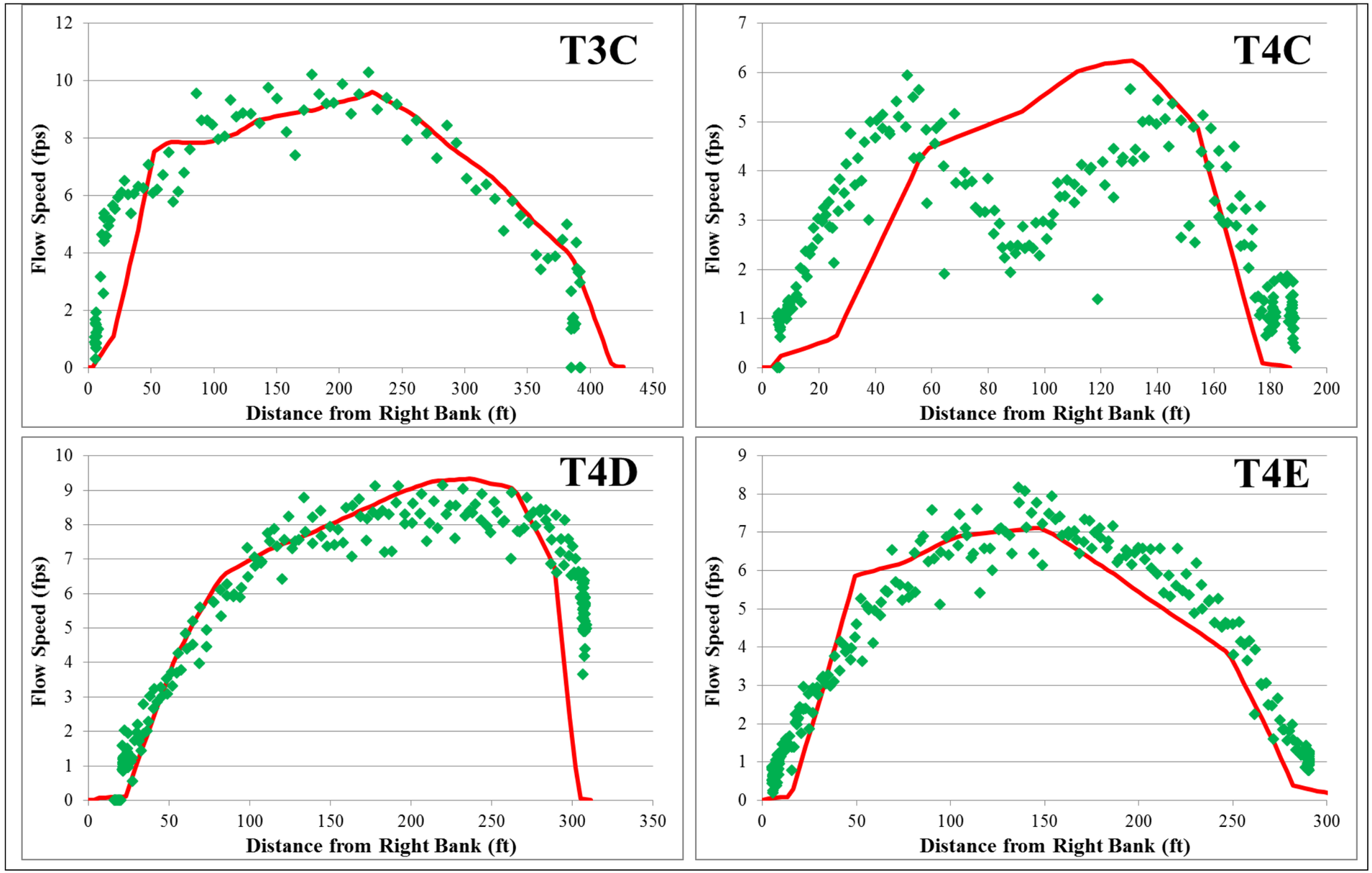

Figure 19: Slough 8A Creek Complex (FA-128) Cross-channel velocity transects measured by boat-mounted ADCP on September 10, 2013. Red line is model transect

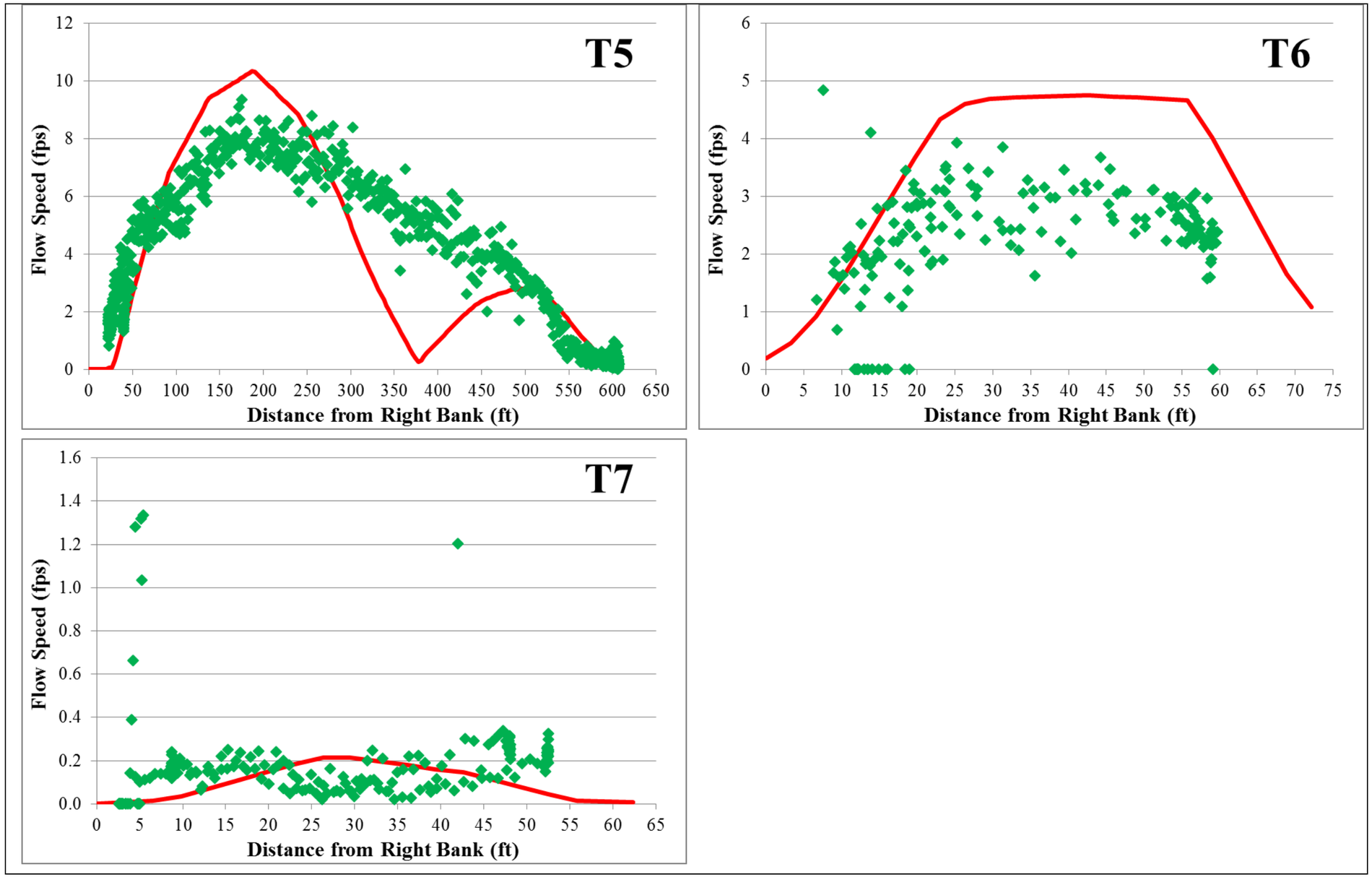

Figure 19. Slough 8A Complex (FA-128) Cross-channel velocity transects measured by boat-mounted ADCP on September 10, 2013. Red line is model transect